

Effect of process parameters on tensile strength of welds and modeling of laser welding of PA6/NBR/clay nanocomposite by response surface methodology

Mohammadreza Nakhaei^{1*}, Ali Ahmadi², Ghasem Naderi³

¹Faculty of Mechanics and Energy, Shahid Beheshti University, Tehran, Iran

²Faculty of Mechanical Eng., Shahid Rajaee Teacher Training University, Tehran, Iran

³Iran Polymer and Petrochemical Institute, Tehran, Iran

Received: 2 November 2019, Accepted: 2 March 2020

ABSTRACT

Polyamide 6 / nitrile butadiene rubber / nanoclay (PA6/NBR/clay) nanocomposite has gathered wide acceptance in industry. Laser welding, as a fabrication method, is applied to welding of polymer nanocomposites. In this study, the input parameters (clay (Closite 30B) content, laser power, scan velocity and stand-off-distance) are varied to achieve the best responses (tensile strength of welds). Response surface methodology (RSM) is utilized to investigate the effect of input parameters on mechanical properties. Morphology and tensile properties of nanocomposites were observed with scan electron microscopy (SEM), transmission electron microscopy (TEM) and tensile test. The results demonstrated that increasing the clay content from 1 to 5%wt and stand-off-distance from 4 to 8 mm decreased tensile strength of welds about 15% and 5%, respectively. The tensile strength of PA6/NBR composite is 25.6, whereas the prediction models showed that under optimal conditions of laser power of 105 W, scan velocity of 300 mm/min and stand-off-distance of 4 mm, the maximum tensile strength of PA6/NBR nanocomposite with 1, 3 and 5 % nanoclay are 27.2 MPa, 27.6 MPa and 24.7 MPa, respectively. These tensile strengths are about 99, 89 and 73% of the strength of these nanocomposites before welding. **Polyolefins J (2020) 7: 99-110**

Keywords: PA6/NBR/nanoclay; nanocomposite; laser welding; response surface methodology.

INTRODUCTION

In recent years, polyamide6 (PA6)-based nanocomposites have been applied in various industries. Among the mentioned nanocomposites, PA6/clay has gained considerable attention [1, 2]. This is due to dramatic change in mechanical and thermal properties at very small amount of the clay nanoparticles [2-4]. In other hands, addition of nanoclay fillers to PA6 matrix usu-

ally reduces the toughness of this material. Because an optimum balance of stiffness and toughness is important for some applications, impact modifiers or rubbery materials are added into PA6/clay nanocomposites [5, 6]. Nitrile butadiene rubber (NBR) as an impact modifier is used widely because it enhances impact strength in a wide range of temperatures rather than other rubbers

* Corresponding Author - E-mail: mr_nakhaei@tabriz.ac.ir

[7-9]. So, the mechanical properties of PA6/NBR/clay nanocomposites are balanced and these nanocomposites have achieved widely applications in automotive industries and etc., [10, 11]. To date, morphology, mechanical, physical and other properties of these nanocomposites at different loadings of PA6, NBR and nanoclay have been investigated [12, 13]. The widespread use of these nanocomposites indicates the importance of studying their welding methods.

Last decade, polymer-based nanocomposites are welded with using different methods. Vibration welding of nylon 6 to nylon 66 was studied by Bates et al [14]. They reported that the maximum tensile strength of welds was about 93% and 81% of tensile strength of unwelded PA6 and PA66, respectively. Also, the friction stir welding of PA6 was used by Nandhini et al [15]. They concluded that the rotational speed, feed rate and tool plunge depth are effective on weld strength. Also under optimal conditions of rotational speed of 1200 min^{-1} , tool plunge depth of 2.3 mm and feed rate of 10 mm/min, the maximum of weld strength could be obtained.

The laser welding has been increasingly employed in shipbuilding, automotive and airplane industries [16, 17]. This process has been employed to join different materials including thermoplastics, metals and dissimilar materials because of its advantage such as non-contact, high-quality and pollution-free process [18, 19]. Recently, laser welding of polymer composites and nanocomposites has been studied by researchers due to various advantages such as high quality, high speed, non-contact and flexible process, low heat input and etc. Chen et al. [20] also studied the effect of carbon black (CB) on transmission laser welding of PA6, polycarbonate (PC) and PA6/glass fiber (GF) composites. They concluded that laser energy is attenuated more rapidly in PA6/GF than in PA6. Also, the absorption coefficient of PC was higher than that of PA6. Nakhaei et al. [3, 17] investigated laser welding of PP/clay nanocomposites. They reported that tensile strength of welds increased in high levels of laser power. Also, increasing of clay nanofillers and laser speed has decreased weld strength.

Response surface methodology (RSM) is a set of mathematical and statistical techniques which employ linear or square polynomial functions to describe a sys-

tem and explore experimental conditions in order to discover the best conditions to optimize the outputs [21]. One of the great advantages of RSM is the reduction of the total required numbers of experiments for a system in which the mutual interactions of variables are being analyzed [22, 23]. This method has been widely applied to optimize several responses in the welding of polymer composite studies in which there are different material or procedural input process parameters contributing to responses [17, 24, 25].

It is evident from the literature that the clay content and laser welding process parameters have outstanding effect on weld strength, and finding optimal processing parameters is essential to obtain excellent welds.

In this paper, the effect of clay content and key CO_2 laser welding parameters (i.e.: laser power, welding speed and stand-off-distance) on tensile strength of butt-joint welds (output response) in PA6/NBR/clay nanocomposites is investigated. Also, optimal response surface methodology (RSM), as one of the best optimization techniques, is used to analysis and predict the input parameters affecting weld quality.

METHODOLOGY

Response surface methodology

Response surface methodology is a collection of mathematical and statistical techniques that relates response variables to set of input controllable variables. This technique presents set of experiments based on input control variables and their levels. After determining responses of each set variables (experiments), RSM develops an appropriate mathematical model with nearest fits to response. So, this model can predict response for any set of factors (in the range of selected input variables). Also, this model can specify the optimal input variables leading to optimized response. Usually, a second-order polynomial Eq. (1) is used in RSM [23, 26]:

$$y = \beta_0 + \sum_{i=1}^k \beta_i x_i + \sum_{i=1}^k \beta_{ii} x_i^2 + \sum_{i=1}^{k-1} \sum_{j=2}^k \beta_{ij} x_i x_j + \varepsilon \quad (1)$$

Where k represents the number of variables, x_i and x_j

are the variables. Also β_p , β_{ii} and β_{ij} are called the regression coefficient, β_0 is a constant parameter and ϵ is the residual associated with the experiments.

Experimental design and procedure

The experiments were designed based on a four-factor three levels Box-Behnken design with 5 replications of the central point. The input variable parameters are laser power (P), scan velocity (V), stand-off-distance (S) and clay content (C). The schematic of process parameters is shown in Figure 1. A several number of trial runs were applied to explore the space limits of laser welding parameters. This aim was obtained by cleaning one of the factors at constant values of other factors. The absence of any visible defects such as overheating, decomposition of weld seam and depth of penetration was the criteria for establishing the working ranges of each process parameters. Level of the clay content was selected (1-5) wt.%. The seam weld of the acceptable samples is shown in Figure 2. The level of the selected independent input variables with their ranges and notations are presented in Table 1. The design expert V7 was used to establish the design matrix. To avoid any systematic error, tests were randomly performed as shown in Table 2. RSM is utilized to analyze the experimental data and present the best model based on the experimental response data using the same software. Also, the statistical significant of the model terms was verified using the sequential F-test, lack-of-fit and other adequacy measures with the same software to achieve the best model [4, 26].

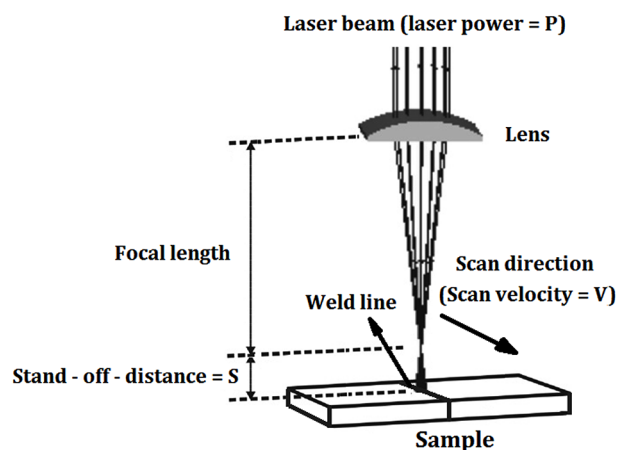


Figure 1. Schematic of process parameters.

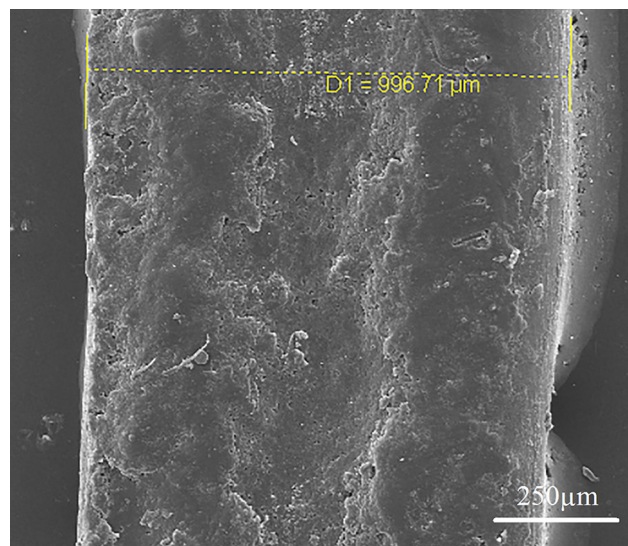


Figure 2. SEM micrograph of the acceptable seam weld of a joint.

EXPERIMENTAL

Material

PA6, NBR and nanoclay were supplied by Kolon Plastic Co. of Korea, Korea Kumho Polychem and Southern Clay, respectively. The nanoclay used in the nanocomposite was Cloisite 30B. Table 3 presents the detailed characteristics of the raw materials used in the nanocomposites.

Nanocomposite preparation

Nanocomposites of PA6/NBR/nanoclay were prepared in a Haake internal mixer (Germany) for 8 minutes at a temperature of 230°C and rotor speed of 80 rpm. PA6/NBR/clay nanocomposite samples with 1, 3 and 5 wt% the clay content were coded TPO1, TPO3 and TPO5, respectively. The amount (content) of PA6/NBR in samples was fixed at 70/30 (wt/wt). After mixing the materials in the internal mixer, they were hot pressed at 230°C for 10 min, using a Mini Test Press operating at 130 MPa to achieve work piece sheets of 200×160×3.2 mm.

Table 1. Selected input variables and their limits.

Parameters	Units	Notations	Limits		
			-1	0	+1
Clay	Wt%	C	1	3	5
Laser power	Watt	P	80	100	120
Scan velocity	mm/min	V	300	600	900
Stand-off-distance	mm	S	4	6	8

Table 2. Design matrix and the measured response.

Run order	Std order	Input parameter level				Measured output
		C (wt%)	P (watt)	V (mm/min)	S (mm)	Tensile strength (MPa) ± Standard deviation
1	9	3	100	600	6	25.7 ± 0.8
2	15	3	100	900	4	23.0 ± 0.4
3	19	1	100	600	8	24.8 ± 0.9
4	28	3	100	600	6	25.8 ± 0.5
5	22	1	80	600	6	22.0 ± 1.1
6	29	5	80	600	6	18.4 ± 0.6
7	16	3	120	900	6	22.3 ± 0.2
8	25	3	80	600	8	21.9 ± 1.0
9	8	5	100	600	8	22.6 ± 0.4
10	13	3	80	600	4	24.5 ± 0.7
11	24	5	120	600	6	22.0 ± 1.2
12	26	5	100	600	4	23.2 ± 0.5
13	23	5	100	300	6	22.5 ± 0.6
14	17	3	100	300	4	27.9 ± 0.4
15	14	3	100	300	8	23.9 ± 1.3
16	11	3	120	300	6	24.9 ± 0.7
17	21	3	80	300	6	20.1 ± 0.5
18	1	1	100	300	6	25.9 ± 0.3
19	6	3	100	600	6	26.0 ± 0.9
20	12	3	80	900	6	22.2 ± 0.4
21	2	3	100	600	6	25.9 ± 0.2
22	7	1	120	600	6	24.0 ± 1.1
23	20	5	100	900	6	21.5 ± 0.6
24	27	1	100	600	4	25.1 ± 0.4
25	18	1	100	900	6	24.6 ± 0.8
26	3	3	100	900	8	24.4 ± 1.2
27	10	3	120	600	4	24.5 ± 0.3
28	5	3	100	600	6	25.8 ± 1.0
29	4	3	120	600	6	24.8 ± 0.6

Nanocomposite laser welding

A CO₂ laser with a maximum power of 120 w and 1060nm wavelength was used. In order to contact between sheets and their clamp under pressure during the butt-weld, a fixture was used (Figure 3).

Characterization

Tensile strength of the samples was carried out according to ASTM D638 [27] by a Zuker tensile test machine (Zwick co., Germany) at a cross head speed of 1mm/min. The measured responses (strength) are average of at least three tests that are presented in Table 2. Also, the tensile strength of base materials was measured according to standard D638. The tests were

Table 3. Properties of raw materials used in preparation of nanocomposites.

Sample code	PA6/NBR	TPO1	TPO3	TPO5
Tensile strength (MPa)	25.6	27.3	30.8	33.4

performed three times and the average of results and standard deviations are presented in Table 2.

The morphology of weld surfaces of the nanocomposites was observed by scanning electron microscopy (SEM) at room temperature with a Philips XL30

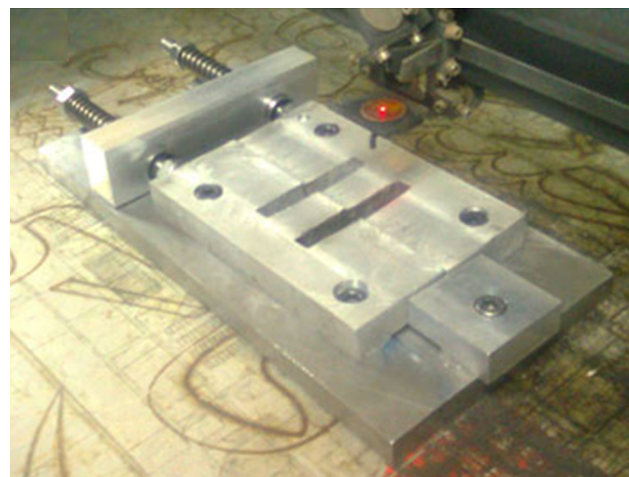
**Figure 3.** Fixture for making pressure during welding operation.

Table 4. Tensile strength of pristine TPO nanocomposites.

Sample code	PA6/NBR	TPO1	TPO3	TPO5
Tensile strength (MPa)	25.6	27.3	30.8	33.4

SEM. The samples were previously coated with a conductive gold thin layer.

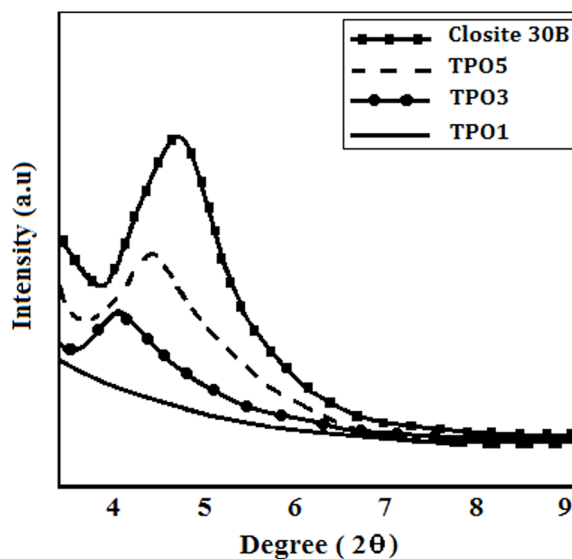
An X-ray diffraction (XRD) equipment was employed to evaluate the dispersion of nanoclay in the PA6/NBR matrix. Analysis by XRD was performed at room temperature on a Philips model X'Pert diffractometer using $\text{CuK}\alpha$ radiation (wavelength $\lambda=1.540598 \text{ \AA}$) generated at 50 kV and 40 mA. The scanning rate was $1^\circ/\text{min}$ in wide angle mode for the 2θ range from 0 to 10° .

To evaluate the dispersion of nanoclay in the nanocomposites, transmission electron microscopy (TEM) with an accelerating voltage of 100 kV was used by a Philips EM208S. Ultra-thin sections were cryogenically cut with a diamond knife at a temperature of -100°C .

RESULTS AND DISCUSSION

XRD analysis

The results of X-ray diffraction of nanocomposites and cloisite 30B are shown in Figure 4. The neat nanoclay exhibits an intensive peak at $2\theta = 4.76^\circ$ (18.54 Å), while the diffraction peaks (interlayer distance) of nanocomposites with 5 and 3 % nanoclay have shifted to lower angles of 4.42° (19.96 Å) and 4.01° (21.95 Å), respectively. The lower diffraction angle of the nanocomposites in comparison with that of the clay shows the polymer chains are intercalated between the layers of the clay [28]. However for TPE nanocomposite with 1 wt. % nanoclay, the characteristic peak of the nanoclay disappeared. The absence of the

**Figure 4.** XRD patterns of Cloisite 30B, TPO1, TPO3 and TPO5 nanocomposites.

diffraction peak shows the exfoliation of the nanoclay into the PA6/NBR matrix.

Development and selection of the response model

Design expert v7 software was applied for analysis experimental data and fitted the best model on the responses. The software suggests the highest order polynomial along with significant terms and the model is not aliased as shown in Table 5(a). Also, Table 5(b) recommends the model with the highest R-squared and predicted R-squared. So, a quadratic model can be used to fit on tensile strength and further analysis. The adequacy of the model was tested using F-test, lack-of-fit test and the analysis-of-variance (ANOVA) technique [26]. The ANOVA table of the quadratic model is shown in Table 6. ANOVA implies that the F-value of this tensile strength model is 17.96, indicating the model is significant. This "model F-value" occurs due to noise with a chance of only 0.01%. The model terms are significant when the values of

Table 5(a). Sequential model sum of squares.

Source	Sum of Squares	df	Mean Square	F Value	p-value Prob > F
Mean vs Total	1643.52	1	1643.52		
Linear vs Mean	44.35	4	11.09	3.68	0.0178
2FI vs Linear	15.62	6	2.60	0.83	0.5640
Quadratic vs 2FI	<u>50.49</u>	<u>4</u>	<u>12.62</u>	<u>28.74</u>	<u>< 0.0001</u>
Cubic vs Quadratic	4.09	8	0.51	1.49	0.3238
Residual	2.06	6	0.34		
Total	16538.13	29	570.63		

Table 5 (b). Model summary statistics.

Source	Std. Dev.	R ²	Adjusted R ²	Predicted R ²	PRESS	
Linear	1.74	0.3803	0.2770	0.1171	102.96	Suggested Aliased
2FI	1.77	0.5142	0.2444	-0.2119	141.32	
Quadratic	0.66	0.9473	0.8945	0.7981	35.20	
Cubic	0.59	0.9823	0.9174	-1.4839	289.64	

"P>F" is less than 0.05 [29]. It is seen from Table 6 that in this experiment, all the input parameters and their interaction such as PV, PS, VS and C², P², V² are significant model terms. The model terms are not significant when the values are greater than 0.05. In this case CP, CV, CS and S² are not significant terms, and they can be eliminated from the model. Further, Table 5 (b) shows the predicted R² and adjusted R² for this model which are 79% and 89%, respectively, and are in reasonable agreement. Finally, the mathematical model for estimation of tensile strength of weld joint within determined design space is presented in below:

a) In terms of coded factors

$$\text{Tensile strength (MPa)} = 25.84 - 1.36 \times C + 1.12 \times P - 0.61 \times V - 0.48 \times S - 1.17 \times P \times V + 0.73 \times P \times S + 1.35 \times V \times S - 1.71 \times C^2 - 2.35 \times P^2 - 0.89 \times V^2 \quad (2)$$

b) In terms of actual factors

$$\text{Tensile strength (MPa)} = -30.75 - 0.9 \times C + 1.2 \times P + 0.015 \times V - 3.42 \times S - 1.95 \times 10^{-4} \times P \times V + 0.018 \times P \times S +$$

$$2.25 \times 10^{-3} \times V \times S - 0.43 \times C^2 - 5.87 \times 10^{-3} \times P^2 - 9.85 \times 10^{-6} \times V^2 \quad (3)$$

Validation of the developed model

Three confirmation experiments were conducted using new test conditions which input variable parameters were chosen randomly from the design matrix. The actual responses were the average of three measured results and the predicted response values were calculated by substituting the input parameters into the developed model. Table 7 shows the new input parameters, the actual experiment, the predicted responses and percentage of error. Figure 5 shows plot of actual vs. predicted strength weld response that the data points are close to the 45° line. Table 7 and Fig. 5 demonstrate that the developed model is quite accurate because the percentage of error between experimental values and the estimated values is small.

Effect of process parameters on weld strength

Perturbation plot is presented in Figure 6. This plot compares the effect of all factors at a center point in

Table 6. ANOVA analysis for the weld tensile model.

Source	Sum of Squares	df	Mean Square	F - Value	p-value Prob > F	Significant
Model	110.46	14	7.89	17.96	<0.0001	*
Clay	22.14	1	22.14	50.41	<0.0001	*
Laser power	14.96	1	14.96	34.07	<0.0001	*
Scan velocity	4.44	1	4.44	10.11	0.0067	*
Stand-off-distance	2.80	1	2.80	6.38	0.0242	*
C × P	0.64	1	0.64	1.46	0.2474	-
C × V	0.04	1	0.04	0.091	0.7673	-
C × S	0.02	1	0.02	0.051	0.8442	-
P × V	5.54	1	5.54	12.57	0.0032	*
P × S	2.10	1	2.10	4.79	0.0461	*
V × S	7.29	1	7.29	16.60	0.0011	*
C ²	19.00	1	19.00	43.26	<0.0001	*
P ²	35.80	1	35.80	81.49	<0.0001	*
V ²	5.10	1	5.10	11.61	0.0043	*
S ²	0.004	1	0.004	0.009	0.9223	-
Residual	6.15	14	0.44	46.90	0.0010	*
Lack of fit	6.10	10	0.61			
Pure error	0.052	4	0.013			
Cor total	116.61	28				

Table 7. Validation test results.

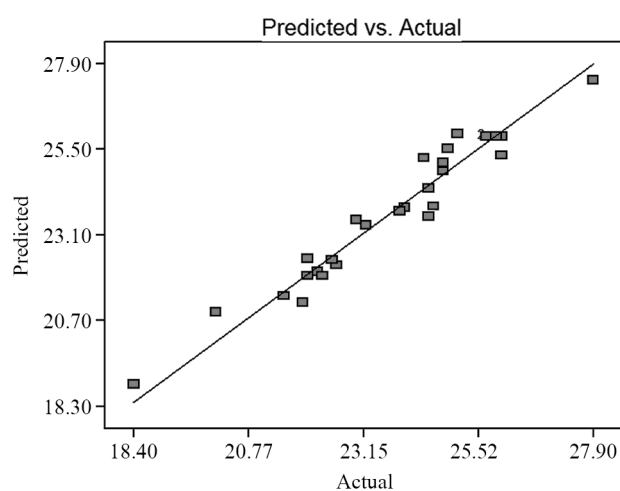
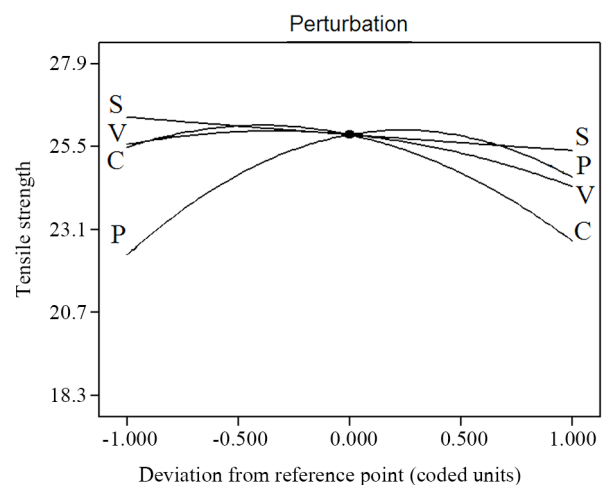
Exp. No.	C (wt. %)	P (watt)	V (mm/min)	S (mm)	Tensile strength (MPa)		
					Actual	Predicted	
1	1	120	400	8	25.1	23.8	5.2
2	3	80	600	6	24.5	22.3	8.9
3	5	100	900	4	18.7	20.6	6.9

the design space. The response is plotted by changing only one factor over its range while the other factors have been held constant. Based on the Figure 6, curvature in the four input factors show that the response (tensile strength) is sensitive to all the input factors [26]. From this figure, it can be noted that the maximum tensile strength of welds is obtained when the laser power is 105 W. It can also be observed that the weld strength decreases with increasing welding speed. This behavior can be explained as following: The tensile strength of welds extensively depends on line energy input (LE) that it is the ratio of laser power (P) per welding speed (V), defined as laser input energy per unit length [3, 17]. Liu et al. [30] and Nakhaei et al. [4] reported the line energy of laser effected on heat input to the base material. They concluded that increasing volume of melted material resulting from the heat input causes a significant enhancement in tensile properties. In the laser power of 105 W and welding speed of 300 mm/min, the line energy is optimum that is desired because more volume of the base mate-

rial is melted, leading to increase in weld strength. At higher level of the speed welding or at the lower level of the laser power, the line energy is very low and thus the heat input to the base material and the volume of melt decreases, consequently the tensile strength of welds decreases. In other hand, high laser power leads to high line energy, so material may be burn and partially decompose as shown in Figure 7, these results are consistent with other reports [3, 31].

It can also be obvious from Figure 6 that stand-off-distance has a slightly negative effect on the tensile strength of welds. This is because decreased power density at high levels of this factor causes low heat input and poor penetration which leads to decreased tensile strength [17, 34]. Acherjee et al. [24] concluded that higher stand-off-distance increases the beam spot diameter at the weld interface. They stated that decreasing beam spot diameter decreases heat input to the base material.

In the case of the clay, increase of clay content of TPO nanocomposite leads to decreasing in tensile strength

**Figure 5.** Plot of actual vs. predicted responses.**Figure 6.** Perturbation plot showing the effect of all input parameters on the response.

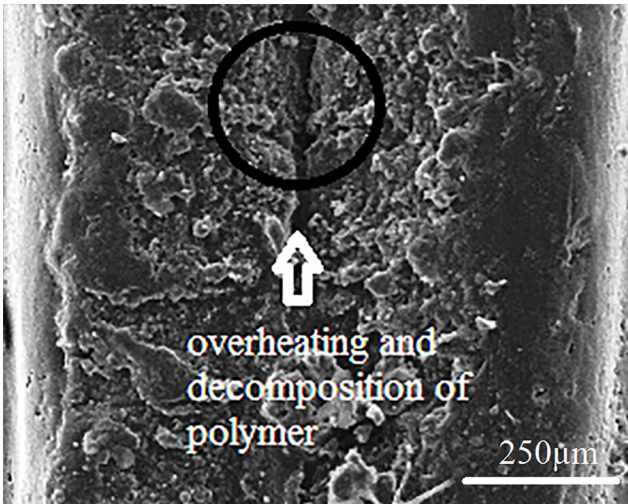


Figure 7. Overheating and decomposition of the weld line at high line energy.

of welds. This behavior can be explained to one of the following reasons. Firstly, the decrease in the surface area for PA6 diffusion at the weld interface, according to literature review [3, 30-32], that makes decreasing of tensile strength of welds. It should be mentioned that good dispersion of the clay content on TPO matrix leads to better weld tensile strength. The degree of dispersion of the cloisite layers within the matrix was studied by TEM. **Figure 8** shows the TEM micrograph of TPO3 nanocomposite. Different magnifications of the micrographs reveal the intercalation and partial exfoliation of the clay in the nanocomposite. In this figure, dark lines represent the cloisite layers

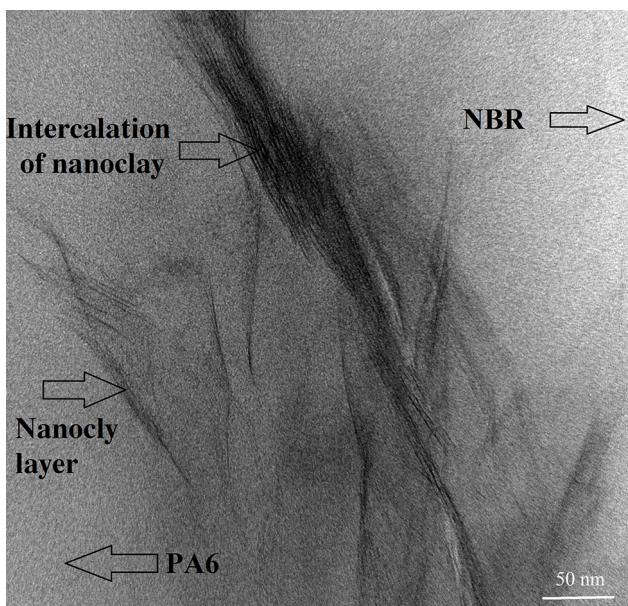


Figure 8. TEM micrograph of PA6/NBR nanocomposite with 3 % Clay.

dispersed within the TPO system.

Figures 9 (a) and (b) show interaction effect of P and V at center values of other factors. The results show that at low power of 80 W, changing in V level has not significant effect on tensile strength. At all level of scan velocity, tensile strength is maximized at laser power of 110 W. In power of 120 W, increasing of speed decreased the tensile strength. This behavior can be due to line energy. In low line energy, low volume of base material could be melted, hence the tensile strength decreased. Also, in high line energy, the base material may be burn and partial decompose, hence the tensile strength decreases. Whereas, appropriate line energy makes maximum tensile strength. Therefore, optimum of laser power with scan velocity (optimum line energy) is desired. Welding in low power with high scan velocity leads to low line energy, and high power with low speed leads to high line energy as discussed ear-

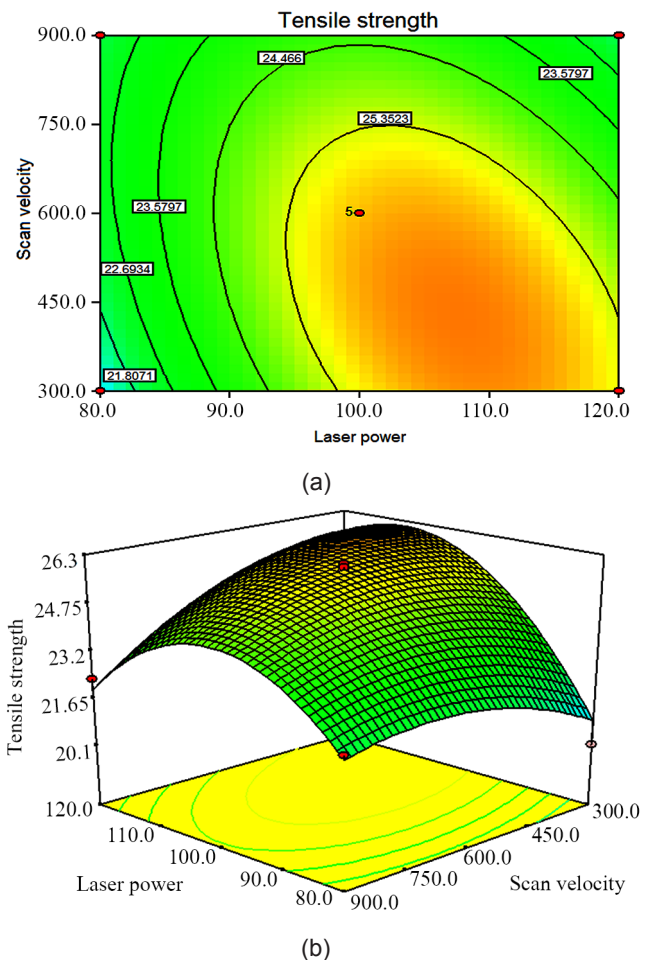


Figure 9. Interaction effect between P and V on response at C = 3%, S=6 mm (a) the contour plot (b) response surface diagram.

lier and stated in [3, 17]. At power of 100-110w, effect of scan velocity is slight, because effect of laser power is more significant than scan velocity. So, the line energy is nearest to optimum condition. Based above results, when clay content and stand-off-distance are kept constant at the center point, the maximum tensile strength of welds (26.2 MPa) can be achieved when the laser power and scan velocity are set to 107 W and 420 mm/min, respectively.

Interaction effect of P and S is presented in Figures 10 (a) and 10(b). It is evident that optimum laser power leads to make the best strength, because at high laser power the base material would burn and partial decompose and at low power density it leads to decrease depth of penetration, hence a weak joint, as discussed in [17, 34]. This figure shows that at low laser power, the tensile strength decreased as the stand-off-distance increased. At higher laser power, effect of stand-off-

distance on tensile strength is lower. This is because at low level of laser power, decreasing stand-off-distance would increase power density but at high level of laser power, the power density is high and decreasing of stand-off-distance could not decrease power density (because the effect of laser power is more than that of stand-off-distance). So, based on the Figures 10 (a) and 10(b), the maximum weld strength (26.3 MPa) is obtained at laser power of 100 W and stand-off-distance of 4 mm.

In relation to interaction V and S that is shown in Figures 11(a) and 11(b), the results indicate that at lowest scan velocity, the tensile strength decreases as stand-off-distance increases, this is due to the defocused laser beam that decreases power density [3, 17]. At the highest scan velocity of 900mm/min, using either a focused or defocused laser beam has no significant effect on tensile strength of welds. This is because the

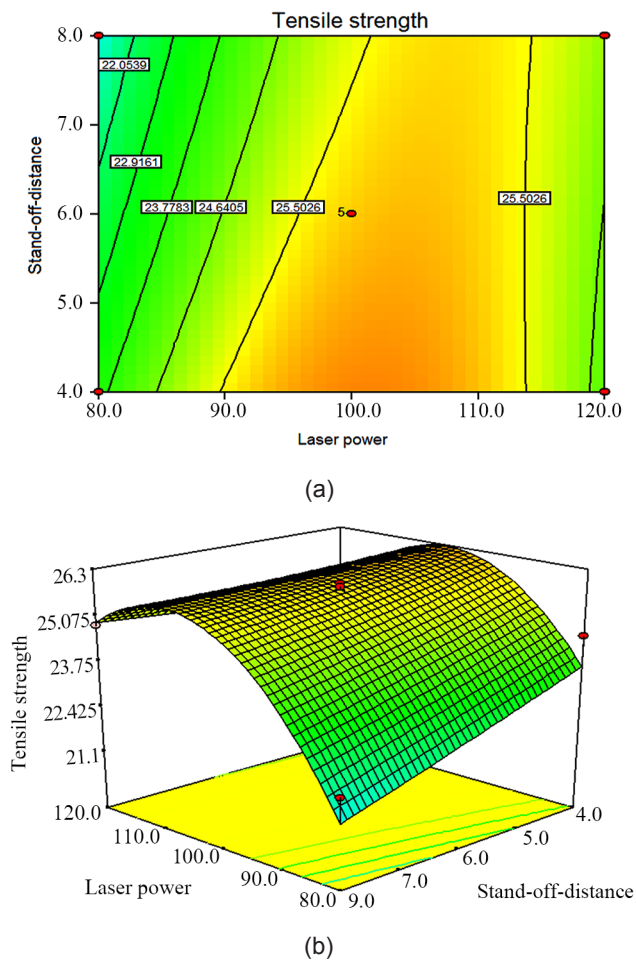


Figure 10. Interaction effect between P and S on response at C = 3%, V=600 mm/min (a) the contour plot (b) response surface diagram.

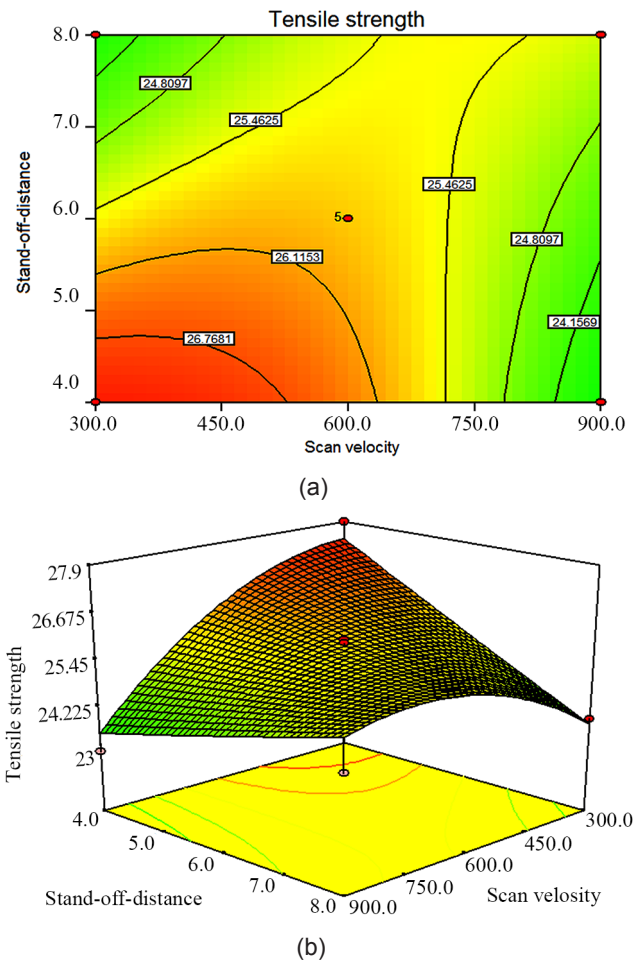


Figure 11. Interaction effect between V and S on response at C = 3%, P=100W (a) the contour plot (b) response surface diagram.

Table 8. Optimal conditions for welding PA6/NBR with 1, 3 and 5 wt% nanoclay.

Exp. No.	C (Wt. %)	P (watt)	V (mm/min)	S (mm)	Tensile strength (MPa)	
					weld	Base material Percentage
1	1	105	300	4	27.2	99.6 %
2	3	105	300	4	27.6	89.6 %
3	5	105	300	4	24.7	73.9 %

scan velocity is more effective than stand-off-distance on the tensile strength. So, at high level of scan velocity, power density is very low, even a focused laser beam cannot be addressed this issue. Based on above discussion, scan velocity of 300-450 mm/min with stand-off-distance of 4-5mm is desired for appropriate welds tensile strength.

For PA6/NBR nanocomposites with 1, 3 and 5% nanoclay, under optimal conditions of laser power of 105 W, scan velocity of 300 mm/min and stand-off-distance of 4 mm, the maximum tensile strength values are 27.2 MPa, 27.6 MPa and 24.7 MPa, respectively. According to Table 8, comparing the weld strength of the three PA6/NBR nanocomposites with tensile strength of the base material shows that the maximum weld strength of TPO1, TPO3, and TPO5 nanocomposites was about 99%, 89% and 73% of the tensile strength of the base material, respectively.

CONCLUSIONS

In this work, effect of clay content and process parameters on CO₂ laser welding of PA6/NBR/clay nanocomposites is studied and the tensile strength of weld joints within input parameters limits is optimized using the RSM. The following results can be extracted from this work:

1. All input parameters have significant effect on response (tensile strength of welds). The clay content, laser power, scan velocity and stand-off-distance have the more effect on response, respectively.
2. The mathematical model conducted from RSM can predict response at 80% confidence level which was fitted to the experimental tests.
3. The maximum tensile strength of welds on TPO1,

TPO3, and TPO5 nanocomposites was about 99%, 89% and 73% of the tensile strength of the base material, respectively.

4. Increasing the clay content from 1 to 5 %wt and stand-off-distance from 4 to 8 mm decreased tensile strength of welds about 15% and 5%, respectively.
5. In terms of interaction of P×V, P×S and V×S, a combination of laser power of 105w, scan velocity of 300 mm/min and stand-off-distance of 4 mm is recommended that leads to maximum weld strength.

REFERENCES

1. Cheremisinoff P (1997). Handbook of engineering polymeric materials CRC Press.
2. Gomari S, Ghasemi I, Karrabi M, Azizi H (2015) An investigation on non-isothermal crystallization behavior and morphology of polyamide 6/ poly (ethylene-co-1-butene)-graft-maleic anhydride/organoclay nanocomposites. Polyolefins J 2: 99-108
3. Nakhaei M, Arab NM, Naderi G, Gollo MH (2013) Experimental study on optimization of CO₂ laser welding parameters for polypropylene-clay nanocomposite welds. J Mech Sci Technol 27: 843-848
4. Nakhaei M, Naderi G, Mostafapour A (2016) Effect of processing parameters on morphology and tensile properties of PP/EPDM/organoclay nanocomposites fabricated by friction stir processing. Iran Polym J 25: 179-191
5. Taghizadeh E, Naderi G, Dubois C (2010) Rheological and morphological properties of PA6/ECO nanocomposites. Rheol acta 49: 1015-

- 1027
6. Mallick S, Kar P, Khatua B (2012) Morphology and properties of nylon 6 and high density polyethylene blends in presence of nanoclay and PE-g-MA. *J Appl Polym Sci* 123: 1801-1811
 7. Chakraborty S, Bandyopadhyay S, Ameta R, Mukhopadhyay R, Deuri A (2007) Application of FTIR in characterization of acrylonitrile-butadiene rubber (nitrile rubber). *Polym Test* 26: 38-41
 8. Fagundes E, Jacobi MA (2012) PA/NBR TPVs: Crosslink system and properties. *Polímeros* 22: 206-212
 9. Mostafapour A, Naderi G, Nakhaei MR (2016) Theoretical models for prediction of mechanical behaviour of the PP/EPDM nanocomposites fabricated by friction stir process. *Polyolefins J* 4: 99-109
 10. Mahallati P, Arefazar A, Naderi G (2011) Thermal and morphological properties of thermoplastic elastomer nanocomposites based on PA6/NBR. *Iran J Chem Eng* 8: 56-65
 11. Oshinski A, Keskkula H, Paul D (1992) Rubber toughening of polyamides with functionalized block copolymers: 2. Nylon-6, 6. *Polymer* 33: 284-293
 12. Paran S, Naderi G, Ghoreishy M (2017) Microstructure and mechanical properties of thermoplastic elastomer nanocomposites based on PA6/NBR/HNT. *Polym Composite* 38: E451-E461
 13. Paran SR, Naderi G, Ghoreishy MR (2016) Effect of halloysite nanotube on microstructure, rheological and mechanical properties of dynamically vulcanized PA6/NBR thermoplastic vulcanizates. *Soft Mater* 14: 127-139
 14. Bates P, Dyck C, Osti M (2004) Vibration welding of nylon 6 to nylon 66. *Polym Eng Sci* 44: 760-771
 15. Nandhini R, Moorthy MK, Muthukumaran S (2017) Effect of welding parameters on microstructure and tensile strength of friction stir welded PA 6, 6 joints. *Int Polym Process* 32: 416-424
 16. Bachmann FG, Russek UA (2002) Laser welding of polymers using high-power diode lasers. In: Photon processing in Microelectronics and Photonics. Proc. SPIE 4637, Photon Processing in Microelectronics and Photonics, (18 June 2002); DOI: 10.1117/12.470660
 17. Nakhaei M, Arab NM, Naderi G (2013) Application of response surface methodology for weld strength prediction in laser welding of polypropylene/clay nanocomposite. *Iran Polym J* 22: 351-360
 18. Mayboudi L, Birk A, Zak G, Bates P (2007) Laser transmission welding of a lap-joint: Thermal imaging observations and three-dimensional finite element modeling. *J Heat Transfer Sep* 129: 1177-1186
 19. Naderi G, Mostafapour A, Nakhaei M (2014) Effect of nanoclay and process parameters on weld strength and seam width for CO₂ laser welding of polypropylene-clay nanocomposite. 11th Seminar on Polymer Science and Thechnology (ISPST), https://www.civiliacom/Paper-ISPST11-ISPST11_133.html
 20. Chen M, Zak G, Bates PJ (2011) Effect of carbon black on light transmission in laser welding of thermoplastics. *J Mater Process Technol* 211: 43-47
 21. Hazrati H, Jahanbakhshi N, Rostamizadeh M (2018) Hydrophilic polypropylene microporous membrane for using in a membrane bioreactor system and optimization of preparation conditions by response surface methodology. *Polyolefins J* 5: 97-109
 22. Nejabat GR, Nekoomanesh M, Arabi H, Sahebi MH, Zohuri GH, Mortazavi SMM, Ahmadjo S, Miller SA (2015) Study of Ziegler-Natta/(2-PhInd) 2ZrCl₂ hybrid catalysts performance in slurry propylene polymerization. *Polyolefins J* 2: 73-87
 23. Mostafapour A, Akbari A, Nakhaei M (2017) Application of response surface methodology for optimization of pulsating blank holder parameters in deep drawing process of Al 1050 rectangular parts. *Int J Adv Manufact Technol* 91: 731-737
 24. Acherjee B, Kuar AS, Mitra S, Misra D (2012) Modeling and analysis of simultaneous laser transmission welding of polycarbonates using

- an FEM and RSM combined approach. *Opt Las Technol* 44: 995-1006
25. Kumar N, Bandyopadhyay A (2017) Simulation of the effects of input parameters on weld quality in laser transmission welding (LTW) using a combined response surface methodology (RSM)-finite element method (FEM) approach. *Lasers in Eng* 36: 225–243
 26. Nakhaei MR, Mostafapour A, Naderi G (2017) Optimization of mechanical properties of PP/EPDM/clay nanocomposite fabricated by friction stir processing with response surface methodology and neural networks. *Polym Composite* 38: E421-E432
 27. Taghizadeh E, Naderi G, Razavi-Nouri M (2011) Effects of organoclay on the mechanical properties and microstructure of PA6/ECO blend. *Polym Test* 30: 327-334
 28. Hajiabdolrasouli M, Babaei A (2018) Rheological, thermal and tensile properties of PE/nanoclay nanocomposites and PE/nanoclay nanocomposite cast films. *Polyolefins J* 5: 47-58
 29. Mostafapour A, Naderi G, Nakhaei MR (2018) Effect of process parameters on fracture toughness of PP/EPDM/nanoclay nanocomposite fabricated by novel method of heat assisted Friction stir processing. *Polym Composite* 39: 2336-2346
 30. Bani Mostafa Arab N (2015) Investigation on tensile strength of friction stir welded joints in pp/epdm/clay nanocomposites. *Int J Eng* 28: 1382-1391
 31. Ahmadi A, Arab NM, Naderi G, Nakhaei M (2017) Optimization of CO₂ laser welding process parameters of PP/EPDM/Clay nanocomposite using response surface methodology. *Mech Ind* 18: 220
 32. Mokhtarzadeh A and Benatar A (2004) Experiments in hot plate welding of polypropylene nanocomposite. *ANTEC*: 1168- 1172
 33. Ghorbel E, Casalino G, Abed S (2009) Laser diode transmission welding of polypropylene: Geometrical and microstructure characterisation of weld. *Mater Des* 30: 2745-2751
 34. Nonhof C (1994) Laser welding of polymers. *Polym Eng Sci* 34: 1547-1549